JOURNAL OF SOLID STATE CHEMISTRY 98, 252–262 (1992)

Ionic Configuration of Copper Ferrimanganites $Cu_{0.5}Mn_xFe_{2.5-x}O_4$

M. LENGLET, J. KASPEREK, B. HANNOYER,* AND J. LOPITAUX

Laboratoire de Physicochimie des Matériaux, I.N.S.A. de Rouen, B.P. 8, 76131 Mont Saint Aignan Cedex, France

A. D'HUYSSER

Laboratoire de Catalyse Hétérogène et Homogène URA 402-Université Lille I, 59655 Villeneuve d'Ascq Cedex, France

AND J. C. TELLIER

I. U. T. d'Amiens, Département Génie Mécanique et Productique, 80025 Amiens Cedex, France

Received March 22, 1991; in revised form November 25, 1991

Mössbauer spectrometry, neutron diffraction, XANES, and XPS have led to the determination of the cation distributions of the system $Cu_{0.5}Mn_xFe_{2.5-x}O_4$ ($0 \leq x \leq 1.5$). The three cations are present in both tetrahedral and octahedral sites, and the relative number of Fe ions on A- and B-sites remains nearly constant in the whole range of x. It appears that for $x \leq 0.5$ manganese is divalent and copper is in its two oxidation states. For $x > 0.5$ copper and iron are respectively divalent and trivalent; the manganese is in +2 and +3 oxydation states.

I. Introduction

The investigation of ferrites containing manganese and copper ions is very interesting because the three ions can adopt more than one valence state. The problem is the determination of the valencies and the cation distribution of the ferrites in the system $Cu_{0.5}Mn_xFe_{2.5-x}O_4$ ($0 \leq x \leq 1.5$) among the two spinel sublattices. The electrical properties of the copper–manganese ferrites series have been extensively studied, but this paper is the first one devoted to the determination of electronic structure.

* To whom correspondence should be addressed.

II. Experimental Procedure

The preparation of the different $Cu_{0.5}Mn_xFe_{2.5-x}O_4$ compositions was made by the usual oxide-sintering method with CuO, αFe_2O_3, and MnO. The latter oxide was freshly prepared from the calcination of $MnCO_3$ under H_2 at 900°C. After dry mixing of the starting oxides, the mixture was annealed under vacuum in fused silica container: 4 days at 1123 K and 48 h at 1423 K. Finally, the powder in its container was rapidly quenched in isopentane liquid bath. The X-ray powder diagrams showed that all the samples have the same cubic spinel phase with no evidence of separate phases.

0022-4596/92 $5.00

Mössbauer spectra were recorded at room temperature or at 200 K in an external longitudinal magnetic field of 6 T. The spectrometer was calibrated at 300 K with standard iron foil using ^{57}Co in Rh matrix. The spectra were fitted with Lorentzian-shaped lines by the method of least-squares.

The neutron diffraction patterns of $x = 1$ and $x = 1.5$ were recorded respectively at 573 K and 473 K; these temperatures were chosen to suppress the magnetic contribution to the Bragg reflection intensity. The wavelength of the monochromatic neutrons was 0.246 nm.

X-ray photoelectron spectra were recorded at room temperature ($p < 10^{-8}$ mm Hg) on a Leybold Heraeus LHS 10 spectrometer with $AlK_{\alpha,1,2}$ X-ray excitation (1486.6 eV). All binding energies were referenced to the C (1*s*) peak of pollution carbon at 285 eV.

III. Experimental Results

Mössbauer Study

Figure 1 shows the Mössbauer spectra for various compositions at room temperature. The hyperfine spectra are split into six broad and unresolved absorption lines. They are attributed to the superposition of several sextets arising from the presence of multiple hyperfine fields at Fe nuclei on the B-sites. With an increase in manganese content the evolution of the broad and asymmetric lines is characteristic of a decrease in Fe^{2+} ions content (*1*, *2*). The spectra of the compound $x = 0$ have already been studied (*1*, *2*). $Cu_{0.5}Fe_{2.5}O_4$ has narrow A-site lines with typical Fe^{3+} parameters. Its B-site lines, asymmetrically broadened, show a large spreading toward zero fields, and the fit has required the superposition of two field-distributions (one with a ferric-like isomer shift and the other one with an isomer shift attributed to an average iron). The study of $Cu_xFe_{3-x}O_4$ compounds (*1*, *2*) has demonstrated that a fit with one sextet for tetrahedral iron and a distribution of hyperfine fields for octahedral iron (components having same adjustable isomer shift) already gives interesting information.

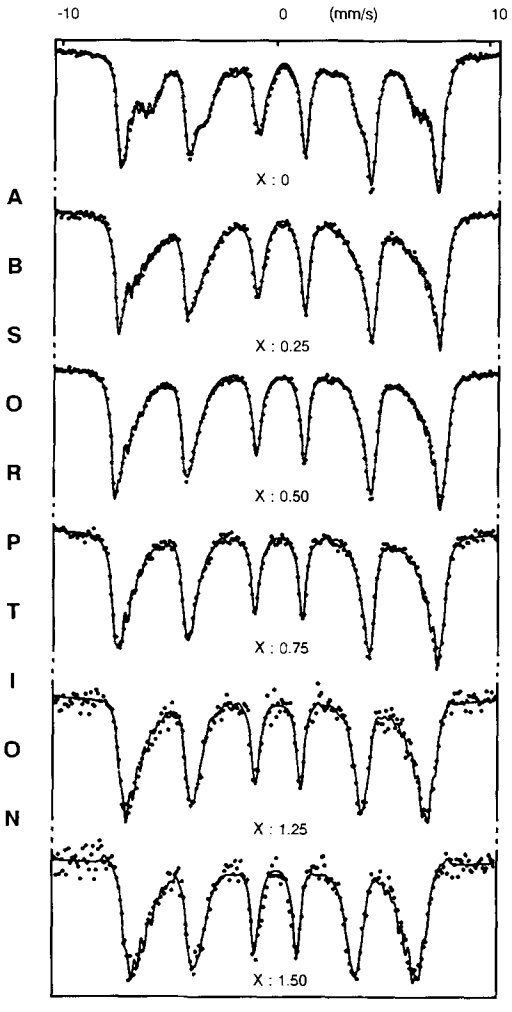

FIG. 1. Mössbauer spectra at room temperature of $Cu_{0.5}Mn_xFe_{2.5-x}O_4$ compounds.

The most interesting hyperfine parameters obtained by fitting the experimental spectra in this way are given in Table I. The spectra of Fe on the B-sites are distributed over 300 or 400 Koe (step of 20 Koe). The full curve on Fig. 1 represents the least-

TABLE I

SUMMARY OF EXPERIMENTAL RESULTS FROM THE MÖSSBAUER SPECTRA

x	T_C (K)	Temp. (K)	δ_A (mm/sec)	$\delta_B - \delta_A$[a] (mm/sec)	Hi_A (Koe)	Γ_A (mm/sec)	S_A (%)
0	625	300	0.25	0.17	462	0.41	27.1
		300(10 T)(2)	0.34	0.16	462	0.48	27.0
0.25	619	300	0.27	0.11	468	0.46	30.9
0.50	609	300	0.28	0.07	472	0.50	31.6
		200(6 T)	0.33	0.12	506	0.44	27.8
0.75	593	300	0.29	0.06	469	0.52	32.5
1	545	300	0.27	0.07	458	0.55	32.8
		200(6 T)	0.32	0.13	494	0.47	31.7
1.25	495	300	0.28	0.07	439	0.59	31.4
1.50	460	300	0.28	0.06	418	0.62	31.6

Note. T_c, Curie temperature; δ, isomer shift relative to Fe–metal at RT; Γ, full width at half maximum; S, area.
[a] Each octahedral component has the same adjustable isomer shift.

squares fit of the experimental spectra; the experimental points are represented by circles.

In order to ensure that the results of such a fit are significant, the A- and B-sextets of the compounds $x = 0.5$ and $x = 1$ have been separated under an external magnetic field of 6 T applied parallel to the direction of γ-ray. Spectra are presented in Fig. 2. The

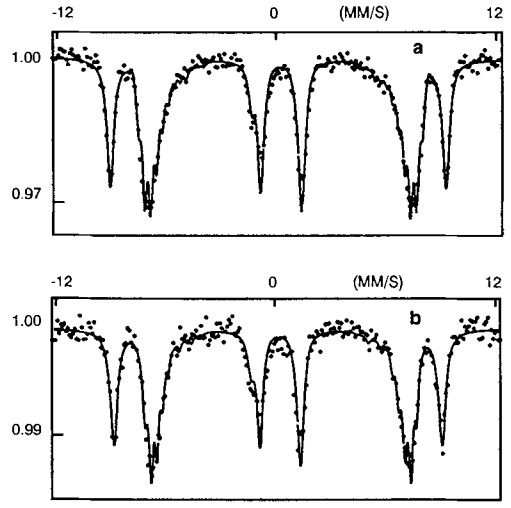

FIG. 2. Mössbauer spectra at 200 K, under applied field of 6 T parallel to the γ-beam: (a) $Cu_{0.5}Fe_2Mn_{0.5}O_4$; (b) $Cu_{0.5}Fe_{1.5}Mn_xO_4$.

outermost pattern is related to the ferric ions on the A-sites and the inner patterns arise from the ferric ions on the B-sites. The large linewidth of the B-site pattern confirms the existence of various supertransferred hyperfine field contributions from the neighboring sites.

In spite of the difficulty in distinguishing very low Fe^{2+} ion concentrations in such spinels, no B-site Fe^{2+} ions are detected. Internal magnetic fields, isomer shifts, and areas are listed in Table I and fit well with the former results obtained without field at 300 K.

The observed effective hyperfine fields and the absence of $\Delta m = 0$ lines, are in agreement with the assumption of a collinear, Neel-type spin structure.

The internal magnetic field H_{iA} at 300 K increases with the decrease in the concentration of iron up to $x = 0.5$ then decreases as rapidly as the Curie temperature (Fig. 3); this is compatible with a decrease in A-site Cu^+ ions content up to $x = 0.5$, because the nonmagnetic Cu^+ ions modify the exchange interaction (*1, 2*). The A-site Fe^{3+} isomer shift, δ_A, is found to be nearly the same for all the compositions. On the other hand, the isomer shift of each component of the B-site

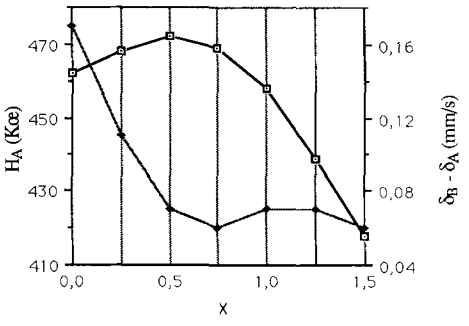

FIG. 3. A site hyperfine fields (□) and variation between A-site and B-site isomer shift (◆) at room temperature.

field distribution decreases along with the decrease in concentration of iron up to $x = 0.5$ (Fig. 3); this is in agreement with the complete disappearance of Fe^{2+} ions from $x = 0.5$ and with the occupation of octahedral sites by Fe^{3+} ions.

Assuming the recoilless fraction of Fe^{3+} ions at A- and B-sites to be equal, the relative number of these ions is determined by the areas under the resolved spectra due to these ions. Areas for $x > 1$ are not accurate enough to take into consideration the possible influence of the Jahn–Teller Mn^{3+} ions on the recoilless fraction. The percentage of the total iron present on the A-sites is indicated in Table I. The variation of S_A is not significant, so it is reasonable to conclude that for $0 < x < 1.5$, about 30% of the iron goes to the A-sites and that 70% goes to the B-sites.

On the basis of the Mössbauer results, without external applied field, Gupta *et al.* (*3*), suggested the cation distribution of the compound $x = 0.5$ as $Fe^{3+}[Cu^{+}_{0.5}Mn^{3+}_{0.5}Fe^{3+}]O_4$. They did not detect Fe^{2+} ions, however, their distribution of Fe^{3+} ions on the two sites is not consistent with the results of this study. Nevertheless, the lack of information about the heat treatment of the samples cannot allow a quantitative comparison.

Neutron Diffraction Study

For the cation distribution, the distinction can be made between neighboring elements from the neutron diffraction intensity data. In the present study, the scattering amplitude of the manganese ($b = -0.36 \times 10^{-12}$ cm) is quite different from that of iron ($b = 0.96 \times 10^{-12}$ cm) and that of copper ($b = 0.76 \times 10^{-12}$ cm).

Since the compounds are ferrimagnetic, at room temperature, the neutron diffraction spectra have been observed above the Curie temperature and therefore indicate only the nuclear contribution to the patterns (thermomagnetic analysis reveals reversible Curie temperature for the compounds $Cu_{0.5}Mn_1Fe_{1.5}O_4$ and $Cu_{0.5}Mn_{1.5}Fe_1O_4$, so the cation distribution and valence states remain unchanged in the range 273–573 K).

When the iron is substituted by the manganese in $Cu_{0.5}Mn_xFe_{2.5-x}O_4$ ($x = 1$; $x = 1.5$) (Fig. 4) the intensity of the (222) reflection, which is sensitive to the cations in B-sites, is varying; this variation shows that a more important fraction of the octahedral sites are occupied by Mn.

The intensity of the (220) and (422) reflections, sensitive to the cations in A-sites, remains unchanged and therefore indicates few changes in the tetrahedral environment. Least-squares refinements with isotropic temperature factors give the cation distributions, which are in Table VII,

$x = 1$

$$Cu^{2+}_{0.05}Mn^{2+}_{0.50}Fe^{3+}_{0.45}[Cu^{2+}_{0.45}Mn^{3+}_{0.50}Fe^{3+}_{1.05}]O_4$$

$x = 1.5$

$$Cu^{2+}_{0.18}Mn^{2+}_{0.50}Fe^{3+}_{0.32}[Cu^{2+}_{0.32}Mn^{3+}_{1}Fe^{3+}_{0.68}]O_4$$

(these results are in excellent agreement with those deduced from other measurements: XPS, XANES, and Mössbauer studies and confirm the conclusion issued from thermomagnetic analysis).

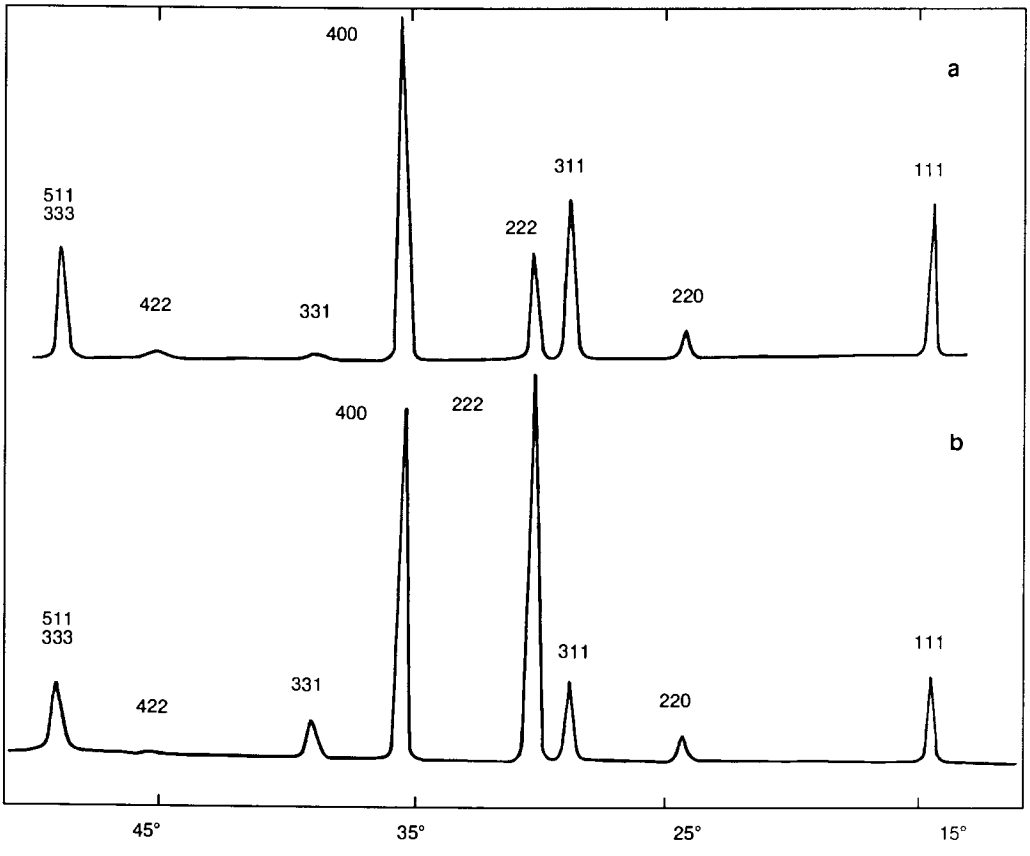

FIG. 4. Neutron diffraction patterns of $Cu_{0.5}Mn_xFe_{2.5-x}O_4$, $\lambda = 0.246$ nm: (a) $x = 1$, $T = 573$ K; (b) $x = 1.5$, $T = 473$ K.

XANES Study

The study of chemical effects in X-ray spectra provides valuable information regarding the electronic structure and bonding in chemical compounds. The measurements of the X-ray absorption spectra were recorded for iron, copper, and manganese in the mixed ferrites with the synchrotron radiation of LURE-DCI (Orsay). The more characteristic *K*-edges are presented in Fig. 5.

From chemical shifts (see Table II), it may be inferred that in the range $0 \leq x < 0.5$ iron and copper are in their two possible oxidation states. For $x > 0.5$, copper and iron are respectively divalent and trivalent.

In conclusion, the copper–manganese ferrites for $x < 0.5$ are iron and copper mixed valence oxides such as the $Cu_xFe_{3-x}O_4$ spinels (*4*, *5*). In $Cu_{0.5}Mn_{0.5}Fe_2O_4$, copper(II) is mainly octahedral.

It had been observed that the chemical shifts of the *K* X-ray absorption discontinuity of manganese depend on various factors like valency, coordination number, and type of chemical bonding, and may be correlated with the effective charge q on the absorption ion in Mn(II) compounds (*6–8*). Experimental data relative to reference compounds and mixed ferrites are listed in Table III.

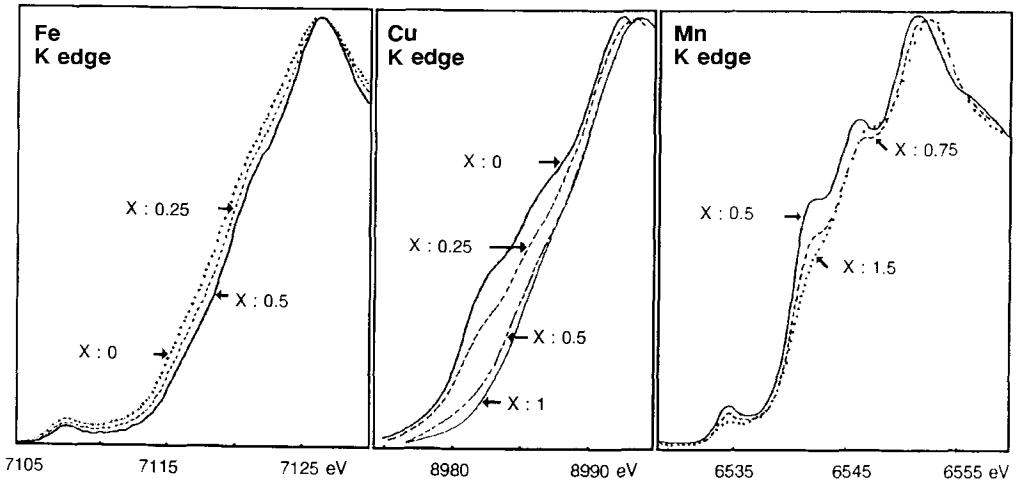

FIG. 5. Fe, Cu, and Mn *K*-XANES in different compounds of the $Cu_{0.5}Mn_xFe_{2.5-x}O_4$ system.

TABLE II

CHEMICAL SHIFTS OF Fe AND Cu *K*-EDGES

	ΔE_K (eV)					
	Reference compounds		$Cu_{0.5}Fe_{2.5-x}Mn_xO_4$			
	$CuFe_2O_4$	Fe_3O_4	$x = 0$	0.25	0.50	0.75
Fe *K*-edge	9.1	7.6	8.5	9	9.4	9.4
Cu *K*-edge	~6		3.5	3.5	~5.75	6

TABLE III

CHEMICAL SHIFTS AND FINE STRUCTURE OF Mn *K*-EDGE XANES

			ΔE_K (eV)	Energy of transitions (eV)		
Reference Compounds	Mn(II)	$MnCr_2O_4$	6.7	7.5	11.6	17.2
		$MnGa_2O_4$	5.9	7.6	10.6	16.8
	Mn(III)	Mn_2O_3	8.2			18.4
		$ZnMn_2O_4$	9.0		13	18.8
		Mn_3O_4	7	8.2	12.7	18.1
$Cu_{0.5}Mn_xFe_{2-x}O_4$ system		$x = 0.5$	6.8	7.8	11.6	16.8
		0.75	6.8			
		1	7.1	7.6	12.3	17.4
		1.25	7.2	7.9	13.1	17.8

XANES of insulating transition metal compounds can be separated into two parts:

(a) the first ~10 eV energy, where the weak features called pre-edge peaks are due to transitions to unoccupied bound antibonding orbitals;
(b) the continuum part, where the peaks have been identified as multiple-scattering resonances due to the plotoelectron sensitive to both coordination geometry and interatomic distances.

Belli *et al.* (*6*) have published a study of Mn *K*-XANES in simple oxides and complex compounds in which the Mn atom is octahedrally coordinated. These authors find good agreement between their experimental NES peak separation and Tossell's calculated MO levels for the Z + 1 cluster $(FeO_6)^{10-}$ (*9*). They assign the NES peaks of the first part of the Mn *K*-edge as follows: the weak pre-edge peaks are transitions to the $2t_{2g}$ and $3e_g$ MO's of primarily Mn 3*d* character, and the pre-edge hump is a transition to the a_{1g}, t_{1u} MO of mostly Mn 4*p* character. The main absorption maximum is not a MO transition but rather a "shape resonance."

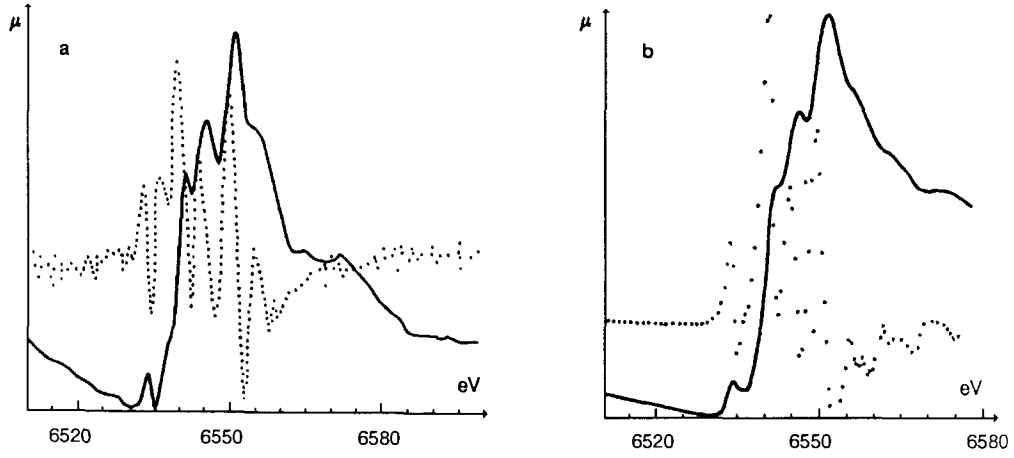

FIG. 6. Mn K-XANES in (a) $MnCr_2O_4$ and (b) $Cu_{0.5}Mn_{0.5}Fe_2O_4$.

The prepeak of Mn(II) in tetrahedral environment is very similar to that of Fe(III) in shape and intensity (see Table IV).

The fine structure of the Mn K-edge spectrum in $Cu_{0.5}Mn_{0.5}Fe_2O_4$ (prepeak and main peak) is quite similar to that of tetrahedral Mn^{2+} in spinels (Fig. 6). The shoulder at 7eV above the prepeak is relative to the $1s \rightarrow 7a_1$, $8t_2$ transition. The broadening of the main peak and the weaker resolution of the spectra for $MnGa_2O_4$ and $Cu_{0.5}Mn_{0.5}Fe_2O_4$ are due to a slight amount of Mn(II) on octahedral sites (20% in $MnGa_2O_4$ and ~10% in $Cu_{0.5}Mn_{0.5}Fe_2O_4$).

For $x > 0.5$, the structures of the continuum part are shifted to higher energy as in Mn_3O_4. These mixed ferrites are manganese mixed valence oxides with Mn(II) tetrahedral and Mn(III) octahedral.

XPS Study

XPS study of copper ferrite spinels $Cu_{1-x}Fe_{2+x}O_4$ ($0 < x \leq 0.5$) gave information about valence states and cationic distribution of copper in matrix spinel (*5*). The copper binding energies reveal that copper is monovalent and divalent and that Cu^{2+} and

TABLE IV

FINE STRUCTURE ANALYSIS OF REFERENCE COMPOUNDS

ion $3d^5$ in Td	Ref.	FWMH (eV)	Decomposition of the pre-edge peak in 2 Lorentzian lines	Parameters of the reference structure[a] $\Delta(^5E - {}^5T_2)$
Fe^{3+}in $NiFeCrO_4$	(*10*)	1.7		0.5 eV
Mn^{2+}in $MnCr_2O_4$	[b]	1.8		to
$MnGa_2O_4$		1.8	energy separation of 0.6 eV	0.7 eV

[a] According the molecular (Z + 1) analogy.
[b] This study.

TABLE V

CHARACTERISTIC XPS PARAMETERS OF COPPER (5)

	Binding energy (eV)	FWMH (eV)	I_S/I_m[a]
Cu^{2+} tetrahedral	936.2 ± 0.2	2.9 ± 0.1	0.85 ± 0.05
Cu^{2+} octahedral	934.0 ± 0.2	2.9 ± 0.1	0.55 ± 0.05
Cu^{+} tetrahedral	932.8 ± 0.2	1.6 ± 0.1	0
Cu^{+} octahedral	931.3 ± 0.2	1.6 ± 0.1	0

[a] Intensity ratio of the satellite to the main line.

Cu^{+} cations are found respectively in the tetrahedral and octahedral O^{2-} anion environments; the characteristic parameters are presented in Table V (no reduction of the Cu^{2+} component in Cu $2p_{3/2}$ spectra has been observed during XPS measurements on the mixed ferrites which are more stable than $Cu_{0.5}Fe_{2.5}O_4$).

In mixed copper–manganese spinels with Mn(III) and Mn(IV), the $2p$ core levels of different copper species showed a negative chemical shift of about 1.5–2eV compared with those in copper ferrites (*11–13*). For $x > 0.5$, copper XPS data (FWHM and I_s/I_m values) show copper(II) mainly in octahedral environment.

In the present study, Mn $2p$, Fe $2p$, Cu $2p_{3/2}$ and O $1s$ lines were recorded for all samples quoted in the introduction ($0 \leq x \leq 1.5$). All determined energy parameters are summarized in Table VI. The Cu $2p_{3/2}$ spectra are shown in Fig. 7.

In the $Cu_{0.5}Mn_xFe_{2.5-x}O_4$ series, the experimental results enable us to draw the following conclusions:

for $x < 0.5$:

(i) the copper is monovalent and divalent: Cu^{+} in octahedral sites (E_B = ~931 eV) and Cu^{2+} mainly octahedral;

(ii) the manganese(II) is tetrahedral.

for $x > 0.5$:

(i) the copper is divalent and mainly octahedral;

(ii) the manganese is in two oxidation states: +2 in tetrahedral sites (satellites at 6–8 eV above the main peak as in $MnCr_2O_4$) and probably +3 in octahedral sites (increase of Δ_E (Mn $2p_{3/2}$–O $1s$)).

From the foregoing results (XPS and XANES), the ionic configuration of $Cu_{0.5}Mn_{0.5}Fe_2O_4$ can be deduced to be

$$Cu_a^{2+}Mn_{0.45}^{2+}Fe_{0.55-a}^{3+}[Cu_{0.5-a}^{2+}Mn_{0.05}^{2+}Fe_{1.45+a}^{3+}]O_4^{2-} \quad a \sim 0.05.$$

IV. Discussion

The cation distribution deduced from neutron diffraction measurements, Mössbauer, XPS, and XANES studies are shown diagrammatically in Fig. 8.

Šimša and Andrejev (*14*) have studied the electrical properties of copper–manganese ferrites: the electrical resistivity and the Seebeck coefficient were measured in the

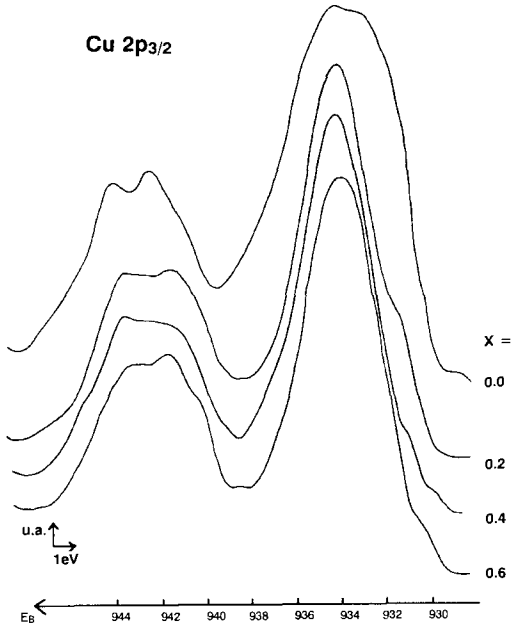

FIG. 7. Cu $2p_{3/2}$ photoelectron spectra in $Cu_{0.5}Fe_{2.5}O_4$ and $Cu_{0.5}Mn_xFe_{2.5-x}O_4$ spinels.

TABLE VI

XPS DATA OF $Cu_{0.5}Fe_{2.5}O_4$ AND MIXED FERRITES

Compound (x =)	Binding energy (eV)						
	Mn $2p_{3/2}$	ΔE (Mn $2p_{3/2}$–O 1s)	Fe $2p_{3/2}$	ΔE (Fe $2p_{3/2}$–O 1s)	Cu $2p_{3/2}$	FWMH	I_s/I_m[b]
0			711.3	181.1	933.8	6.1	0.42
0.2	641.4	111.3	711.3	181.1	934.1–931.5[a]	4.0	
0.25	641.3	111.2	711.3	181.1	933.8	4.4	0.50
0.4	641.5	111.4	711.2	181.0	934.2–931[a]		
0.5	641.7	111.4	711.5	181.3	934.3	4.5	0.57
0.6	641.8	111.5	711.6	181.3	934.3		
0.75	641.6	111.7	711.5	181.6			
1	641.6	111.7	711.6	181.7	934.3	4.8	0.60
1.25	641.7	111.8	711.6	181.7	934.3	4.8	0.60

[a] Shoulder.

[b] Intensity ratio of the satellite to the main line.

temperature range 80–800 K on single crystals and polycristals from the system $Cu_{0.5}Mn_xFe_{2.5-x}O_4$ ($0 \leq x < 1$).

Taking into account the temperature course of ρ and θ and their dependence on the chemical composition the authors concluded that the system studied might be divided into three regions:

for $x < 0.3$, the behavior of the electrical properties is analogous to $Cu_{0.5}Fe_{2.5}O_4$ (*15*, *22*) and manganese ferrites $Mn_{x'}Fe_{3-x'}O_4$, with $x' < 1$, and is characteristic for the simultaneous presence of bi- and trivalent iron ions on the octahedral sites of the spinel lattice.

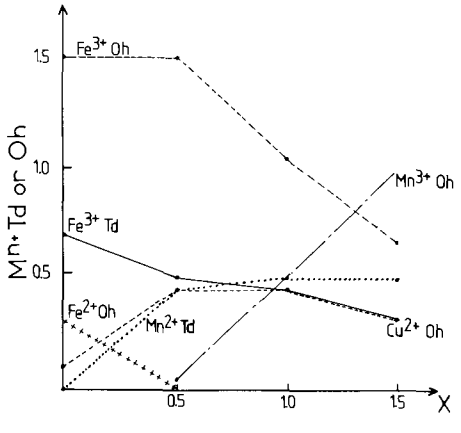

FIG. 8. Cation distribution for $Cu_{0.5}Mn_xFe_{2.5-x}O_4$.

for $0.3 < x < 0.7$, an increase of ρ, θ, and activation energy is observed, but the increase is much slighter than an analogous one in the series of manganese ferrites at $x' = 1$.

for $x > 0.7$, the conduction mechanism is rather different from that observed with manganese ferrites for $x > 1$: the contribution of positive charge carriers is apparent. A similar conduction mechanism has been observed in ferrites close to the copper ferrite $CuFe_2O_4$ (*15*, *16*).

The model established in this study for the cation distribution is in good agreement with the investigation of the electrical properties. By substituting manganese for iron in $Cu_{0.5}Fe_{2.5}O_4$, it can be expected that replacement $Mn^{2+} \rightarrow Fe^{2+}$ will occur first; Mn^{2+} ions mostly enter the tetrahedral positions thus taking the place of copper.

The cation distributions for $0 \leq x \leq 1$ are summarized in Table VII, along with the literature data (for qualitative comparison).

The existence of two solid-state charge transfer redox systems may be postulated in

TABLE VII

CATION DISTRIBUTIONS FOR $Cu_{0.5}Mn_xFe_{2.5-x}O_4$ SYSTEM ISSUED FROM THIS STUDY AND FOUND IN THE LITERATURE

Composition	Cation distribution			Ref.
	Td	Oh		
$Cu_{0.5}Fe_{2.5}O_4$	$Cu^{+}_{0.24}Fe^{3+}_{0.76}$	$[Cu^{2+}_{0.26}Fe^{2+}_{0.26}Fe^{3+}_{1.48}]$	O^{2-}_4	(*17*)
	$Cu^{+}_{0.10}Cu^{2+}_{0.20}Fe^{3+}_{0.70}$	$[Cu^{+}_{0.10}Cu^{2+}_{0.10}Fe^{2+}_{0.30}Fe^{3+}_{1.5}]$	O^{2-}_4	(*2*)
$Cu_{0.5}Mn_{0.3}Fe_{2.2}O_4$	$Cu^{+}_{0.18}Mn^{2+}_{0.24}Fe^{3+}_{0.58}$	$[Cu^{2+}_{0.32}Mn^{3+}_{0.06}Fe^{2+}_{0.08}Fe^{3+}_{1.54}]$	O^{2-}_4	(*14*)
$Cu_{0.5}Mn_{0.5}Fe_2O_5$	$Cu^{+}_{0.08}Mn^{2+}_{0.41}Fe^{3+}_{0.51}$	$[Cu^{2+}_{0.43}Mn^{3+}_{0.08}Fe^{2+}_{0.08}Fe^{3+}_{1.41}]$	O^{2-}_4	(*17*)
	$Cu^{2+}_{0.11}Mn^{2+}_{0.37}Fe^{3+}_{0.52}$	$[Cu^{2+}_{0.39}Mn^{2+}_{0.13}Fe^{3+}_{1.48}]$	O^{2-}_4	(*18*)
	$Cu^{2+}_{0.05}Mn^{2+}_{0.45}Fe^{3+}_{0.50}$	$[Cu^{2+}_{0.45}Mn^{2+}_{0.05}Fe^{3+}_{1.50}]$	O^{2-}_4	This study
$Cu_{0.5}Mn_1Fe_{1.5}O_4$	$Cu^{2+}_{0.05}Mn^{2+}_{0.50}Fe^{3+}_{0.45}$	$[Cu^{2+}_{0.45}Mn^{3+}_{0.50}Fe^{3+}_{1.05}]$	O^{2-}_4	This study
$Cu_{0.5}Mn_{1.5}Fe_1O_4$	$Cu^{2+}_{0.18}Mn^{2+}_{0.50}Fe^{3+}_{0.32}$	$[Cu^{2+}_{0.32}Mn^{3+}_{1}Fe^{3+}_{0.68}]$	O^{2-}_4	This study

order to explain the evolution of the formal valence configuration in the range $0 \leq x \leq 0.5$:

$$Cu^{+} + Fe^{3+} \rightleftarrows Cu^{2+}_{octa} + Fe^{2+}$$

$$Fe^{2+} + Mn^{3+} \rightleftarrows Fe^{3+} + Mn^{2+}_{tetra}.$$

The introduction of Mn^{2+} in tetrahedral sites involves the migration of copper on octahedral sites: the two redox systems are displaced on the right-hand side corresponding to the more stable configuration of the spinel lattice,

$$Mn^{2+}_{tetra} + Fe^{3+}.$$

For $x > 0.5$, copper(II) is mainly octahedral. For still higher manganese content, the concentration of iron(II) drops to zero and manganese(III) replaces iron on octahedral sites. The $Cu^{2+}_{octa} + Mn^{3+}_{octa}$ configuration is stable, unlike the $Cu^{2+}_{tetra} + Mn^{3+}_{octa}$ configuration. In mixed valence copper manganites such as $CuMn_2O_4$ (*19, 20, 13,*) and $CuMn_{2-x}M_xO_4$ (M = Cr, Fe) (*13, 21*), the redox equilibrium

$$Cu^{+}_{tetra} + Mn^{4+}_{octa} \rightleftarrows Cu^{2+}_{tetra} + Mn^{3+}_{octa}$$

is all the more displaced toward the left-hand side, as the tetrahedral copper concentration is larger.

References

1. B. LEREBOURS, J. DÜRR, A. D'HUYSSER, J. P. BONNELLE, AND M. LENGLET, *Phys. Status Solidi A* **61,** K1 (1980).
2. B. HANNOYER AND M. LENGLET, *Stud. Inorg. Chem.* **3,** 617 (1983); B. HANNOYER, Thèse doctorat d'état, Rouen (1983).
3. M. P. GUPTA, S. BADRINARYANAN, AND A. P. B. SINHA, *Indian J. Chem.* **19,** 894 (1980).
4. B. HANNOYER, J. DURR, G. CALAS, J. PETIAU, AND M. LENGLET, *Mater. Res. Bull.* **17,** 435 (1982).
5. A. D'HUYSSER, B. HANNOYER, M. LENGLET, AND J. P. BONNELLE, *J. Solid State Chem.* **39,** 246 (1981).
6. M. BELLI, A. SCAFATI, A. BIANCONI, S. MOBILIO, L. PALLADINO, A. REALE, AND E. BURATTINI, *Solid State Commun.* **35,** 355 (1980).
7. M. APTE, C. MANDE, AND J. P. SUCHET, *J. Chim. Phys.* **79,** 325, (1982).
8. M. LENGLET, J. LOPITAUX, AND J. DÜRR, *Mater. Chem. Phys.* **14,** 199, (1986).
9. J. A. TOSSELL, D. J. VAUGHAM, AND K. H. JOHNSON, *Am. Mineral.* **59,** 319, (1974).
10. B. HANNOYER, M. LENGLET, AND J. C. TELLIER, *Rev. Chim. Miner.* **24,** 68 (1987).
11. V. A. M. BRABERS AND F. VAN SETTEN, *J. Phys. D* **16,** L169 (1983).
12. A. D. D. BROEMME AND V. A. M. BRABERS, *Solid State Ionics* **16,** 171 (1985).
13. M. LENGLET, A. D'HUYSSER, J. KASPEREK, J. P. BONNELLE, AND J. DÜRR, *Mater. Res. Bull.* **20,** 745 (1985).
14. Z. ŠIMŠA AND N. ANDREJEV, *Czech. J. Phys.* **B19,** 1389 (1969).

15. C. F. JEFFERSON, *J. Appl. Phys.* **36,** 1165 (1965).
16. M. ROSENBERG, M. NICOLAU, AND P. BUNGET, *Phys. Status Solidi A* **15,** 521 (1966).
17. L. ČERVINKA AND Z. ŠIMŠA, *Czech. J. Phys.* **B20,** 470 (1970).
18. A. NARAYANASAMY AND L. HÄGGSTRÖM, *J. Phys. C* **16,** 591 (1983).
19. N. K. RADHAKRISHNAN AND A. B. BISWA, *Phys. Status Solidi A* **44,** 45 (1977).
20. R. E. VANDERBERGHE, *Phys. Status Solidi A* **50,** K85 (1978).
21. M. LENGLET, P. FOULATIER, J. DÜRR, AND J. ARSENE, *Phys. Status Solidi A* **94,** 461 (1986).
22. L. NAMBA, *J. Appl. Phys.* **49,** 2950 (1978).